A Three-Dimensional Transport Model for Determining Absorbed Fractions of Energy for Electrons Within Cortical Bone

Lionel G. Bouchet and Wesley E. Bolch

Department of Nuclear and Radiological Engineering, University of Florida, Gainesville, Florida

Any radionuclide that is transported through the blood stream will also be carried through the haversian canals within cortical bone. These canals are lined with a layer of endosteum that contains radiosensitive cells. This paper introduces a new three-dimensional electron transport model for cortical bone based on Monte Carlo transport and on bone microstructural information for several cortical bone regions. **Methods:** Previously published haversian cavity and bone matrix chord length distributions for cortical bone were randomly sampled to create alternating regions of bone matrix, endosteum and haversian canal tissues during the three-dimensional transport of single electrons. Electron transport was performed using the EGS4 transport code with the parameter reduced electron step transport algorithm. Electron-absorbed fractions of energy were tabulated for three adult cortical bone sites considering three source and target regions: the cortical haversian space, the cortical bone endosteum (CBE) and the cortical bone volume (CBV). **Results:** Absorbed fractions assessed with the new model were shown to be highly energy dependent for most combinations of source-target regions in cortical bone. Although chord length data were available for three different bone sites (femur, humerus and tibia), very little variation with bone site was noted in the absorbed fraction data. **Conclusion:** International Commission on Radiation Protection (ICRP)-recommended absorbed fractions for cortical bone are given only for the CBE as target region and for the CBE and CBV as source regions. Comparisons of these recommended absorbed fractions with the absorbed fractions calculated in this study show large differences. For example, ratios of self-absorbed fractions to the CBE in this model and in the ICRP 30 model are ~0.25, ~4 and ~1.5 for initial electron energies of 10, 200 keV and 4 MeV, respectively. Consequently, this new transport model of electrons in cortical bone will improve the relatively energy-independent data recommended by the ICRP. This model will also allow consideration of the haversian canals as a potential radiation source.

Key Words: dosimetry; cortical bone; absorbed fractions; Monte Carlo; endosteum; haversian canals; EGS4

J Nucl Med 1999; 40:2115–2124

Received Nov. 12, 1998; revision accepted Jun. 21, 1999.

For correspondence or reprints contact: Wesley E. Bolch, PhD, Department of Nuclear and Radiological Engineering, University of Florida, Gainesville, FL 32611-8300.

The human skeletal system is a complex structure that can be classified in two distinct types: trabecular bone (a spongy mixture of bone spicules and marrow cavities) and cortical bone (hard, dense bone). These two bone types are microscopically quite different and therefore need to be considered separately for dosimetry purposes. Within the skeletal system, the cells at carcinogenic risk have been identified as the hematopoietic stem cells (active bone marrow) and the osteogenic cells, especially those on the endosteal surfaces and certain epithelial cells close to bone surfaces in the head (*1*). In the adult human skeleton, active marrow is located in the trabecular bone regions. Osteogenic cells are found on the surfaces of the trabecular bone cavities and lining the haversian canals within cortical bone. For this reason, trabecular and cortical regions must be considered separately to accurately calculate the dose to the skeletal system. We have recently developed a new three-dimensional transport model for electrons in adult trabecular bone (*2*). In this article, we present a companion transport model for electrons within human adult cortical bone.

Cortical bone is found in the outer wall of all bones and in the shafts of the long bones. This bone structure is composed of tissue units called osteons or haversian systems. The osteon is a cylindric system running approximately parallel to the long axis of the long bones and has at its center the haversian canal. Each canal contains blood vessels, lymphatic nerves and connective tissue and is lined by a layer of endosteum. The haversian canals are linked by transverse Volkmann's canals that connect to sites of bone marrow and to the exterior surface of bone. These canals contain only blood vessels and are fewer in number than the haversian canals. The wall of the osteon consists of concentric bone lamellae (layered bone). Osteons are separated by interstitial lamellae (irregularly shaped systems of lamellar bone) and cement lines. The concentric and interstitial lamellae, as well as the cement lines, are composed of bone matrix, which contains both inorganic and organic components. Typical structural dimensions of the components of the cortical bone are given in Table 1 (*3*).

In cortical bone, the cells at risk with respect to radiation

TABLE 1
Typical Geometric Dimensions of Human Adult Osteon (Haversian System)

Feature	Typical dimensions
Osteon length (between Volkmann canals)	2500 μm
Concentric lamellae thickness	7 μm
Osteon diameter	200–400 μm
Haversian canal diameter	20–200 μm
Endosteum thickness	10 μm

are the osteoprogenitor cells that lie within the 10-μm layer of endosteum (*4*). Therefore, for dosimetric purposes, cortical bone can be considered to consist of the cortical bone matrix (organic and inorganic components and enclosed osteocytes) and the soft tissues of the haversian systems.

In this article, a three-dimensional transport model of electrons in cortical bone is presented. It is based on transverse path-length measurements through haversian canals and the mineralized bone tissue of cortical bone as performed by Beddoe (*3,5*). Absorbed fractions of energy for monoenergetic electron sources are subsequently calculated using the EGS4 parameter reduced electron step transport algorithm (PRESTA) Monte Carlo transport code (*6,7*), considering three cortical bone regions (shaft of femur, tibia and humerus) and all source and target combinations (bone volume, endosteum and other soft tissues within the haversian canals).

PREVIOUS DOSIMETRIC MODELS OF CORTICAL BONE

A.H. Beddoe

In 1976, A.H. Beddoe used a bone scanning microscope to measure transverse chord lengths through haversian cavities and the intervening cortical bone matrix (*3,5*). [In Beddoe's sample preparation procedures, all soft tissues were removed before optical scanning. Consequently, we make a distinction between the haversian cavity (total soft tissue volume defining the haversian canal inclusive of its constituent endosteal layer) and the haversian space (soft tissues within the canal exclusive of the endosteum)]. This bone-scanning microscope was originally developed for path-length measurements in trabecular bone (*8*) and was further refined to measure the small cavities in cortical bone. Stained sections of transverse slices of cortical bone (20–30 μm thick) were scanned to obtain transverse chord length distributions of the haversian cavity sizes and cortical bone matrix, the latter defined as the distances between haversian cavities in the plan perpendicular to the bone axis. With this optical scanning system, an effective resolution of about 8 μm was achieved. The transverse chord length distributions obtained by Beddoe are shown on the two graphs of Figure 1 for the cortical cavities and the mineralized component. Beddoe made measurements of the cortex in three cortical bones: the humerus, the tibia and the femur. In these measurements, he assumed that the haversian cavities ran parallel to the long axis of the bone, which is generally the case for the long bones. He also assumed that the number of transverse canals (Volkmann's canals) appearing in the transverse planes was negligibly small. This last assumption was verified visually on stained sections of cortical bones. Beddoe also looked at the iliac crest, but his measurements showed irregular fluctuations caused by scanning only one small section. Average transverse chord lengths for these three long bones are given in Table 2.

Beddoe followed the technique used by Whitwell (*9*) and Whitwell and Spiers (*9,10*) for the dosimetry of trabecular bone, also using Whitwell's cortical chord length measurements. This technique assumes a straight path of the electron through haversian cavities and cortical bone matrix and uses a range-energy relationship with random sampling of chords to derive dose conversion factors. These dose conversion factors were published only in Beddoe's dissertation (*3*) and only for a limited number of radionuclides used in health physics (^{14}C, ^{18}F, ^{22}Na, ^{32}P, ^{45}Ca, ^{90}Sr and ^{90}Y). Moreover, the only source considered in his study was the bone volume. However, both the endosteum and haversian canals are of interest for nuclear medicine and health physics dosimetric applications.

G. Akabani

Another study on cortical bone dosimetry was performed by Akabani in 1993 (*11*). He calculated absorbed fractions of energy to single haversian canals and derived dose factors for several β-emitting radionuclides (^{32}P, ^{45}Ca, ^{89}Sr, ^{90}Sr, ^{90}Y, ^{131}I and ^{153}Sm). This single haversian canal was modeled as a cylinder surrounded by a cortical bone matrix. Six haversian canal sizes were considered, with radii of 5, 10, 20, 30, 40 and 50 μm. The Monte Carlo transport code EGS4-PRESTA was used to derive electron absorbed fractions of energy for two sources (haversian canal and bone surface) and three targets (haversian canal, endosteum and bone matrix). From these calculations, dose conversion factors were tabulated for these seven radionuclides as a function of the haversian canal radius.

There are two limitations to this work. The first is that a single radius of the haversian canal was used without considering a distribution of radii. Second, because the average transverse distance between haversian canals is approximately 900 μm (*4,5*) and the range of a 500-keV electron through bone is about 1000 μm (*12*), cross-osteon irradiation should be considered for electron energies greater than 500 keV.

MATERIALS AND METHODS

The model of electron transport in cortical bone presented here attempts to account for the limitations of the two previous cortical bone models (*3,11*) by considering the nonlinear trajectory of the electrons, the full transport of the electrons with δ-rays and

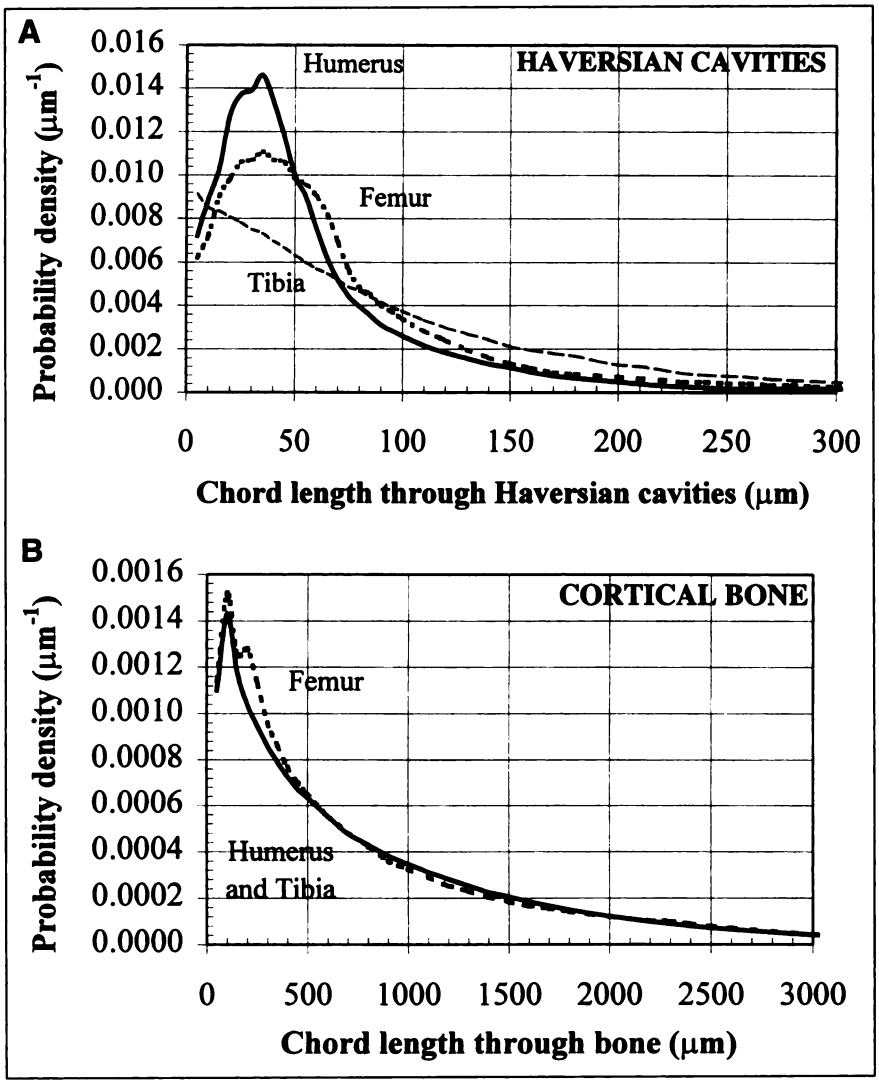

FIGURE 1. Transverse path length distributions of haversian cavities (haversian canal and endosteum) and transverse mineralized component (distance between cavities) in cortex of femur, tibia and humerus of 50-y-old man (*3,5*).

bremsstrahlung, the distribution of sizes of haversian canals and the cross-osteon irradiation.

The transverse chord length distributions measured by Beddoe (*3,5*) through cortical cavities and cortical bone matrix are used for this model, because they currently give the most complete information on the microstructure of adult cortical bone. They are used following the methodology proposed by Bouchet et al. (*2*) in a model of electron transport in trabecular bone. One difference in the models proposed for both trabecular and cortical bone is that the chord length distributions available for the trabecular bone are omnidirectional, whereas for the cortical bone they are transverse (measured within the plane perpendicular to the bone axis).

Transport Model

The transverse chord lengths through haversian cavities and bone matrix are used to limit the transport of the particles in a given region. In the transport model, they represent the distance in the transverse plane between two different cortical bone regions and, in this respect, may be used to determine the change in region during

TABLE 2
Calculated Average Transverse Chord Lengths Through Haversian Cavities and Through Cortical Bone Matrix of Three Different Cortical Bone Sites

Cortical bone site	Average transverse chord (μm)*		% volume of bone matrix†
	Haversian cavities	Bone matrix	
Femur cortex	78	856	93.4
Tibia cortex	100	870	94.6
Humerus cortex	78	870	95.4

*Original transverse chord length data were not available. Consequently, these distributions were graphically estimated from figures given in original thesis (*4*). For these reasons, averages given in this table differ slightly from published values (*3,5*).

†The percentage bone volume calculated by Beddoe (*3,5*).

particle transport. By sampling many different chords, for many electrons, the average transport of an electron in cortical bone is thus simulated.

Another characteristic we know about the cortical bone is that the haversian cavities (the haversian space and its surrounding endosteum) constitute cylinders running parallel to the long axis of the bone, with diameters ~100 times smaller than their lengths (Table 1). Consequently, in the transport model, all regions are represented by parallel portions of cylinders. The escape of the particle from the cortical bone is not simulated; therefore, these cylinders are not limited by any planes along the direction of their axes.

In the transport model, a transverse chord length is randomly sampled each time an electron enters a new region. This chord length gives the distance in the transverse plane between the particle entry points of the new region and the succeeding region. Thus, particle transport is limited by a cylinder centered at the point of entry and of a radius given by the sampled chord length. To take into account possible backscattering of the particle, only half a cylinder is used, with its cutting plane defined by the initial direction of travel of the particle. Figure 2A shows a diagram of this transport geometry.

The chord length distributions are available for only the haversian cavities and cortical bone matrix. The cavities include the haversian space and the surrounding 10-μm cell layer of endosteum (*1,13*). To derive corresponding chord lengths for the endosteum layers and the haversian space, it can be assumed that in the transverse plane the direction of entry in both endosteal layers is isotropic. Mathematically, this corresponds to selecting randomly the angle of entry in the transverse plane θ_1 and θ_2 in both endosteal layers. [The selection of endosteal chord lengths in the haversian canal of cortical bone is performed differently from that for endosteum lining the marrow cavities of trabecular bone (*2*). In the latter, it was assumed that the direction of entry to an endosteum region was isotropic, mathematically leading to the random selection of the cosine of the entry angle. For haversian canals in cortical bone, it is assumed that the direction of entry in the transverse plane is isotropic, mathematically leading to the random selection of the angle of entry in that plane.] Then, because the thickness of the endosteal layer is fixed, the transverse chords for both endosteal layers can be derived:

$$d_{E1} = (10\ \mu m)\sec(\theta_1) \text{ and} \qquad \text{Eq. 1}$$

$$d_{E2} = (10\ \mu m)\sec(\theta_2). \qquad \text{Eq. 2}$$

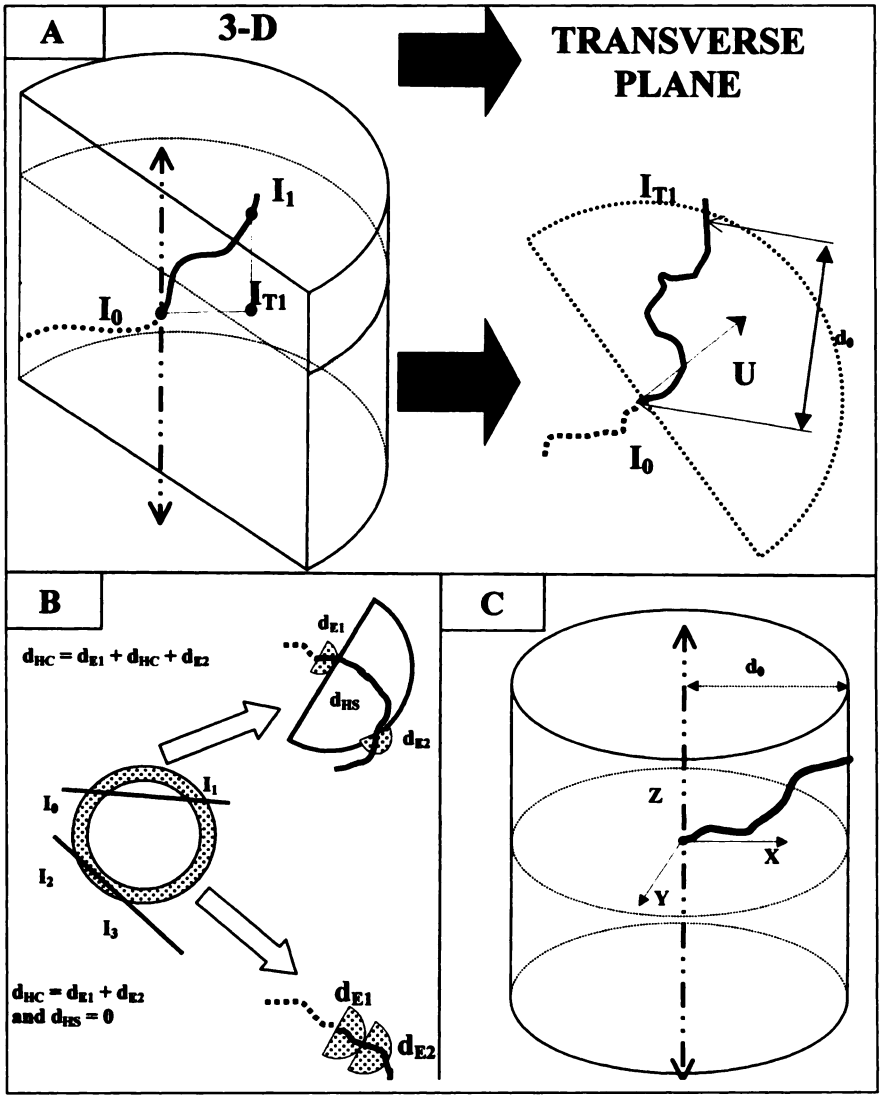

FIGURE 2. Diagrams illustrating model of electron transport in cortical bone. (A) Use of transverse chord lengths to limit transport in transverse plane using half cylinders. In this graph, electron enters at I_0 and exits at I_1. In transverse plane, distance (I_0, I_{T1}) is equal to sampled chord length d_0. (B) Use of measured haversian cavity chords (I_0–I_3) to derive endosteum chord lengths (d_{E1} and d_{E2}) and haversian space chord length (d_{HS}). (C) Cylindric source region in cortical bone derived from l-random chord length distributions.

Therefore, to derive transverse chords for the endosteal layers and the haversian space, a random haversian cavity chord d_{HC} is first sampled along with two endosteum entry angles θ_1 and θ_2. Next, both transverse chords through the endosteum d_{E1} and d_{E2} and through the haversian space d_{HS} can be derived as follows:

$$\text{if } d_{E1} + d_{E2} \geq d_{HC}, \text{ then}$$

$$d_{E1} = d_{E2} = \frac{d_{HC}}{2}, \text{ and}$$

$$d_{HS} = 0. \qquad \text{Eq. 3}$$

$$\text{Otherwise if } d_{E1} + d_{E2} \leq d_{HC}, \text{ then}$$

$$d_{E1} = (10\ \mu\text{m})\sec(\theta_1),$$

$$d_{E2} = (10\ \mu\text{m})\sec(\theta_2) \text{ and}$$

$$d_{HS} = d_{HC} - (d_{E1} + d_{E2}). \qquad \text{Eq. 4}$$

Figure 2B shows how these three transverse chords are derived and used in the transport model.

The determination of the starting region must be considered separately. The measurements of transverse chord length distributions in cortical bone performed by Beddoe (*3*) were made under a μ-random distribution, meaning that a chord is defined by a random point in space and a random direction (*14–16*). To simulate a particle originating within the haversian space or within the bone matrix, one must use an I-random distribution, where a chord is defined by a point interior to the region and a given direction. To derive an I-random chord distribution from a μ-random chord distribution, the following relationship can be used:

$$f_I(d) = \frac{d}{\langle d \rangle_\mu} f_\mu(d), \qquad \text{Eq. 5}$$

where $f_I(d)$ and $f_\mu(d)$ are the probability density functions for chord lengths under I and μ randomness, respectively, and $\langle d \rangle_\mu$ is the average chord length under μ randomness (*14*). Thus, using this derived I-random chord distribution, an interior chord length d_I can be derived for both haversian spaces and cortical bone matrix. After choosing an interior chord d_I, a starting internal distance d_0 between 0 and d_I is randomly selected. This selected distance limits the distance traveled in the transverse plane by the electron in the initial source region. In this case, the starting electron is placed at the origin of the coordinate system on a cylinder axis of radius d_0, and its starting direction is selected randomly. This places the electron at a distance d_0 in the transverse plane from the next region but allows the electron to travel in the three dimensions. Figure 2C shows a diagram of the starting source region. In the case of a source taken in the haversian space, two random angles of entry through both endosteal layers are selected, and the corresponding distances decrease the sampled transverse interior chord for the haversian cavity.

In the case of the endosteum as a source, an approximate radius of a cavity cylinder containing the endosteum is derived. This is used only to take into account the relatively large curvature of the endosteum surfaces caused by the small size of the haversian cavities. This radius is derived by randomly sampling a transverse chord length d through the haversian cavities and by assuming that this chord is the average chord $\langle d \rangle$ of a disk of radius R (*14*):

$$\langle d \rangle = \frac{4}{\pi} R. \qquad \text{Eq. 6}$$

From this expression, a cylinder of radius R is created, and a random point is selected within a 10-μm distance from its edge. When the electron exits the starting endosteal region, the method of region creation presented above is used. Note that the original cylinder is never used as a transport region.

Figure 3 summarizes in diagram form the presented model of electron transport in cortical bone. The haversian space is considered the source, and a backscattered electron is shown.

Transport Parameters

The EGS4 Monte Carlo transport code (*7*), along with the PRESTA algorithm (*6*), is used to simulate the transport of the electrons within cortical bone. The composition of each of the cortical bone regions was derived from International Commission on Radiation Units and Measurements (ICRU) report 46 (*17*). The composition of the haversian space was taken as blood, the endosteum as soft tissue and the bone matrix as cortical bone. We acknowledge that the ICRU composition of cortical bone does include the constituent tissues of the haversian space; nevertheless, these tissues compose only a small fraction of the cortical bone volume. Table 3 gives the percentage by mass and density of each medium.

The other transport parameters used for the EGS4 code are a cutoff value for both electron kinetic energy and photon energy equal to 1 keV and an ESTEPE of 2% (maximum percent energy loss per step in the continuous slowing-down approximation). Bremsstrahlung photons are followed up to a distance not to exceed 5 cm from the center of the original region. Twelve electron energies are simulated between 10 keV and 4 MeV, with a total of 20,000 sampled particles per energy. The energy deposited in all cortical bone regions is stored, and absorbed fractions are derived for the cortical haversian space (CHS), the cortical bone endosteum (CBE) and the cortical bone volume (CBV) as source and target regions. Corresponding SDs of the absorbed fraction are also derived for all source, target and energy combinations.

RESULTS AND DISCUSSION

Electron-absorbed fractions of energy are calculated for the three cortical bone sites measured by Beddoe (*3,5*). The results of absorbed fractions for all target regions are given in Table 4 for the CHS as a source, Table 5 for the CBE as a source, and Table 6 for the CBV as a source. Along with the absorbed fractions for each cortical bone site are given the average values for all three sites. This average absorbed fraction is to be used for other cortical bones from which the chord length distributions are not available. The calculated coefficients of variation (CVs) are less than 0.5% when the source and the target region are equal. When the source and target are different, CVs are generally less than 5%, except at very low energies (10, 15 and 20 keV), for which some CVs are as high as 50%.

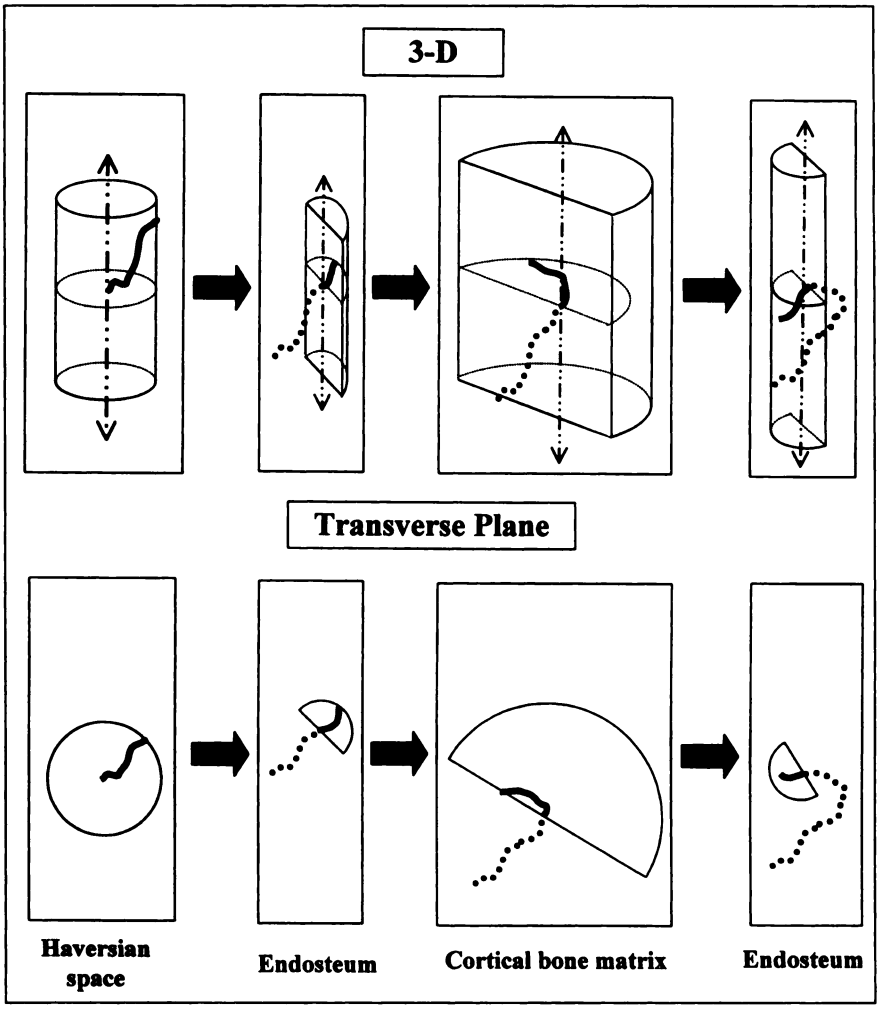

FIGURE 3. Model of electron transport in cortical bone. Source is haversian space, and therefore random chord length is sampled from I-random distribution. After exiting source region, electron enters endosteum region at random angle. Then, electron enters bone matrix and backscatters into endosteum layer. Both three-dimensional (3-D) and transverse diagrams are shown.

TABLE 3
Elemental Composition (% by Mass) of Different Media Used for Simulation of Electron Transport in Cortical Bone*

Element	Haversian space (blood)	Endosteum (soft tissue)	Bone matrix (cortical bone)
H	10.2	10.5	3.4
C	11.0	25.6	15.5
N	3.3	2.7	4.2
O	74.5	60.2	43.5
Na	0.1	0.1	0.1
Mg	—	—	0.2
P	0.1	0.2	10.3
S	0.2	0.3	0.3
Cl	0.3	0.2	—
K	0.2	0.2	—
Ca	—	—	22.5
Fe	0.1	—	—
Mass density (g/cm^3)	1.06	1.03	1.92

*Derived from (*17*).

Self-Absorbed Fractions of Energy

Graphs of self-absorbed fractions are given in Figure 4 for all three cortical bone regions. There are small variations of the self-absorbed fraction between cortical bone sites because of the small differences in their respective chord length distributions. For all three cortical regions, the self-absorbed fraction decreases with increasing energy. This decrease is more pronounced for the haversian space and the endosteum because of their very small sizes. For the bone matrix, the absorbed fraction is very close to unity because of the very large volume occupied by this region (Table 1). For all regions, the decrease seems to be less abrupt for energies greater than 1 MeV, at which cross-osteon irradiation begins to be significant.

Also shown in Figure 4B are values of absorbed fraction for self-irradiation of the CBE as recommended in International Commission on Radiological Protection (ICRP) publication 30. [The cortical bone model of ICRP publication 30 is used within the internal dose computer code MIRDOSE2. The corresponding model for cortical bone used in MIRDOSE3 has not yet been published.] The ICRP 30

TABLE 4
Absorbed Fractions of Energy for Monoenergetic Electrons Emitted Within Cortical Haversian Space

Energy (MeV)	Femur	Humerus	Tibia	Average
Target = CHS				
0.010	9.61E-01	9.63E-01	9.75E-01	9.66E-01
0.015	9.31E-01	9.33E-01	9.53E-01	9.39E-01
0.020	8.95E-01	9.03E-01	9.33E-01	9.10E-01
0.030	8.21E-01	8.35E-01	8.75E-01	8.44E-01
0.050	6.73E-01	7.10E-01	7.53E-01	7.12E-01
0.100	4.15E-01	4.97E-01	4.80E-01	4.64E-01
0.200	2.03E-01	2.95E-01	2.33E-01	2.44E-01
0.500	7.76E-02	1.17E-01	9.59E-02	9.67E-02
1.000	5.03E-02	6.66E-02	6.28E-02	5.99E-02
1.500	4.04E-02	5.14E-02	5.29E-02	4.83E-02
2.000	3.61E-02	4.46E-02	4.82E-02	4.30E-02
4.000	3.08E-02	3.57E-02	4.22E-02	3.62E-02
Target = CBE				
0.010	3.86E-02	3.66E-02	2.41E-02	3.31E-02
0.015	6.69E-02	6.49E-02	4.51E-02	5.90E-02
0.020	1.01E-01	9.19E-02	6.34E-02	8.53E-02
0.030	1.50E-01	1.34E-01	1.04E-01	1.29E-01
0.050	1.68E-01	1.41E-01	1.29E-01	1.46E-01
0.100	1.08E-01	8.62E-02	1.06E-01	9.99E-02
0.200	5.98E-02	4.90E-02	6.22E-02	5.70E-02
0.500	3.49E-02	3.06E-02	3.54E-02	3.36E-02
1.000	2.82E-02	2.54E-02	2.88E-02	2.75E-02
1.500	2.57E-02	2.32E-02	2.65E-02	2.51E-02
2.000	2.43E-02	2.23E-02	2.52E-02	2.39E-02
4.000	2.27E-02	2.08E-02	2.37E-02	2.24E-02
Target = CBV				
0.010	5.20E-04	4.70E-04	5.26E-04	5.05E-04
0.015	1.84E-03	1.88E-03	2.09E-03	1.93E-03
0.020	4.20E-03	5.05E-03	3.91E-03	4.38E-03
0.030	2.91E-02	3.07E-02	2.15E-02	2.71E-02
0.050	1.59E-01	1.49E-01	1.18E-01	1.42E-01
0.100	4.77E-01	4.16E-01	4.14E-01	4.36E-01
0.200	7.37E-01	6.56E-01	7.04E-01	6.99E-01
0.500	8.86E-01	8.52E-01	8.67E-01	8.68E-01
1.000	9.18E-01	9.05E-01	9.05E-01	9.09E-01
1.500	9.28E-01	9.20E-01	9.15E-01	9.21E-01
2.000	9.32E-01	9.25E-01	9.19E-01	9.25E-01
4.000	9.28E-01	9.25E-01	9.16E-01	9.23E-01

CHS = central haversian space; CBE = cortical bone endosteum; CBV = cortical bone volume.

model assigns an absorbed fraction of 0.25 for mean β energies below 200 keV and an absorbed fraction of 0.015 for mean β energies exceeding 200 keV. The ICRP 30 model is shown to underestimate the absorbed fraction, relative to the present model, at electron energies less than ~60 keV and at energies exceeding 200 keV. Discrepancies at very low energies are attributable to differences in source region definition. In the present model, the endosteum is considered

TABLE 5
Absorbed Fractions of Energy for Monoenergetic Electrons Emitted Within Cortical Bone Endosteum

Energy (MeV)	Femur	Humerus	Tibia	Average
Target = CHS				
0.010	2.68E-02	2.66E-02	2.73E-02	2.69E-02
0.015	5.35E-02	5.07E-02	5.70E-02	5.37E-02
0.020	9.27E-02	8.56E-02	1.00E-01	9.28E-02
0.030	1.56E-01	1.45E-01	1.65E-01	1.55E-01
0.050	1.76E-01	1.49E-01	2.00E-01	1.75E-01
0.100	1.16E-01	9.93E-02	1.57E-01	1.24E-01
0.200	6.91E-02	6.46E-02	9.59E-02	7.65E-02
0.500	4.21E-02	4.07E-02	5.65E-02	4.64E-02
1.000	3.36E-02	3.42E-02	4.63E-02	3.80E-02
1.500	3.01E-02	3.02E-02	4.17E-02	3.40E-02
2.000	2.86E-02	2.92E-02	4.01E-02	3.26E-02
4.000	2.68E-02	2.72E-02	3.83E-02	3.08E-02
Target = CBE				
0.010	9.23E-01	9.21E-01	9.21E-01	9.21E-01
0.015	8.38E-01	8.37E-01	8.37E-01	8.37E-01
0.020	7.23E-01	7.31E-01	7.25E-01	7.26E-01
0.030	5.08E-01	5.07E-01	5.03E-01	5.06E-01
0.050	2.71E-01	2.70E-01	2.62E-01	2.68E-01
0.100	1.10E-01	1.08E-01	1.10E-01	1.09E-01
0.200	5.69E-02	5.31E-02	5.82E-02	5.60E-02
0.500	3.45E-02	3.09E-02	3.49E-02	3.34E-02
1.000	2.83E-02	2.56E-02	2.86E-02	2.75E-02
1.500	2.56E-02	2.31E-02	2.63E-02	2.50E-02
2.000	2.43E-02	2.22E-02	2.48E-02	2.38E-02
4.000	2.25E-02	2.07E-02	2.35E-02	2.22E-02
Target = CBV				
0.010	5.08E-02	5.24E-02	5.19E-02	5.17E-02
0.015	1.09E-01	1.13E-01	1.06E-01	1.09E-01
0.020	1.85E-01	1.83E-01	1.75E-01	1.81E-01
0.030	3.36E-01	3.48E-01	3.33E-01	3.39E-01
0.050	5.53E-01	5.82E-01	5.38E-01	5.58E-01
0.100	7.74E-01	7.93E-01	7.33E-01	7.66E-01
0.200	8.73E-01	8.82E-01	8.46E-01	8.67E-01
0.500	9.22E-01	9.27E-01	9.07E-01	9.18E-01
1.000	9.35E-01	9.37E-01	9.22E-01	9.31E-01
1.500	9.38E-01	9.41E-01	9.26E-01	9.35E-01
2.000	9.40E-01	9.41E-01	9.27E-01	9.36E-01
4.000	9.32E-01	9.33E-01	9.20E-01	9.28E-01

CHS = central haversian space; CBE = cortical bone endosteum; CBV = cortical bone volume.

TABLE 6
Absorbed Fractions of Energy for Monoenergetic Electrons Emitted Within Cortical Bone Volume

Energy (MeV)	Femur	Humerus	Tibia	Average
Target = CHS				
0.010	0.00E+00	0.00E+00	0.00E+00	0.00E+00
0.015	0.00E+00	0.00E+00	0.00E+00	0.00E+00
0.020	0.00E+00	4.16E-05	0.00E+00	1.39E-05
0.030	3.66E-04	3.60E-04	4.09E-04	3.79E-04
0.050	3.41E-03	2.72E-03	3.49E-03	3.21E-03
0.100	1.28E-02	1.03E-02	1.70E-02	1.33E-02
0.200	2.25E-02	1.76E-02	3.17E-02	2.39E-02
0.500	2.57E-02	2.63E-02	3.73E-02	2.98E-02
1.000	2.70E-02	2.63E-02	3.79E-02	3.04E-02
1.500	2.55E-02	2.58E-02	3.65E-02	2.92E-02
2.000	2.50E-02	2.58E-02	3.58E-02	2.89E-02
4.000	2.51E-02	2.62E-02	3.58E-02	2.90E-02
Target = CBE				
0.010	8.88E-04	1.38E-03	1.14E-03	1.14E-03
0.015	1.79E-03	1.92E-03	2.03E-03	1.91E-03
0.020	2.70E-03	3.65E-03	2.84E-03	3.06E-03
0.030	6.22E-03	6.01E-03	5.99E-03	6.08E-03
0.050	1.11E-02	1.12E-02	1.09E-02	1.11E-02
0.100	1.74E-02	1.64E-02	1.73E-02	1.70E-02
0.200	2.12E-02	2.02E-02	2.16E-02	2.10E-02
0.500	2.22E-02	2.10E-02	2.32E-02	2.21E-02
1.000	2.27E-02	2.06E-02	2.37E-02	2.23E-02
1.500	2.14E-02	1.99E-02	2.23E-02	2.12E-02
2.000	2.12E-02	1.98E-02	2.22E-02	2.10E-02
4.000	2.13E-02	1.98E-02	2.23E-02	2.11E-02
Target = CBV				
0.010	9.99E-01	9.99E-01	9.99E-01	9.99E-01
0.015	9.98E-01	9.98E-01	9.98E-01	9.98E-01
0.020	9.97E-01	9.96E-01	9.97E-01	9.97E-01
0.030	9.93E-01	9.94E-01	9.94E-01	9.94E-01
0.050	9.86E-01	9.86E-01	9.86E-01	9.86E-01
0.100	9.70E-01	9.73E-01	9.66E-01	9.70E-01
0.200	9.56E-01	9.62E-01	9.46E-01	9.55E-01
0.500	9.50E-01	9.51E-01	9.38E-01	9.46E-01
1.000	9.47E-01	9.50E-01	9.35E-01	9.44E-01
1.500	9.48E-01	9.48E-01	9.36E-01	9.44E-01
2.000	9.45E-01	9.47E-01	9.34E-01	9.42E-01
4.000	9.35E-01	9.35E-01	9.23E-01	9.31E-01

CHS = central haversian space; CBE = cortical bone endosteum; CBV = cortical bone volume.

as a 10-μm-thick volume source with absorbed fractions close to unity at very low source energies. The ICRP 30 model assumes a true surface source for "surface-seeking" radionuclides in which a larger portion of the emitted energy is lost to the neighboring bone matrix.

Cross-Absorbed Fraction of Energy

Graphs of absorbed fractions when the source is different from the target region are given in Figure 5. In the case of the CHS as the target (Fig. 5A), there are larger variations of the

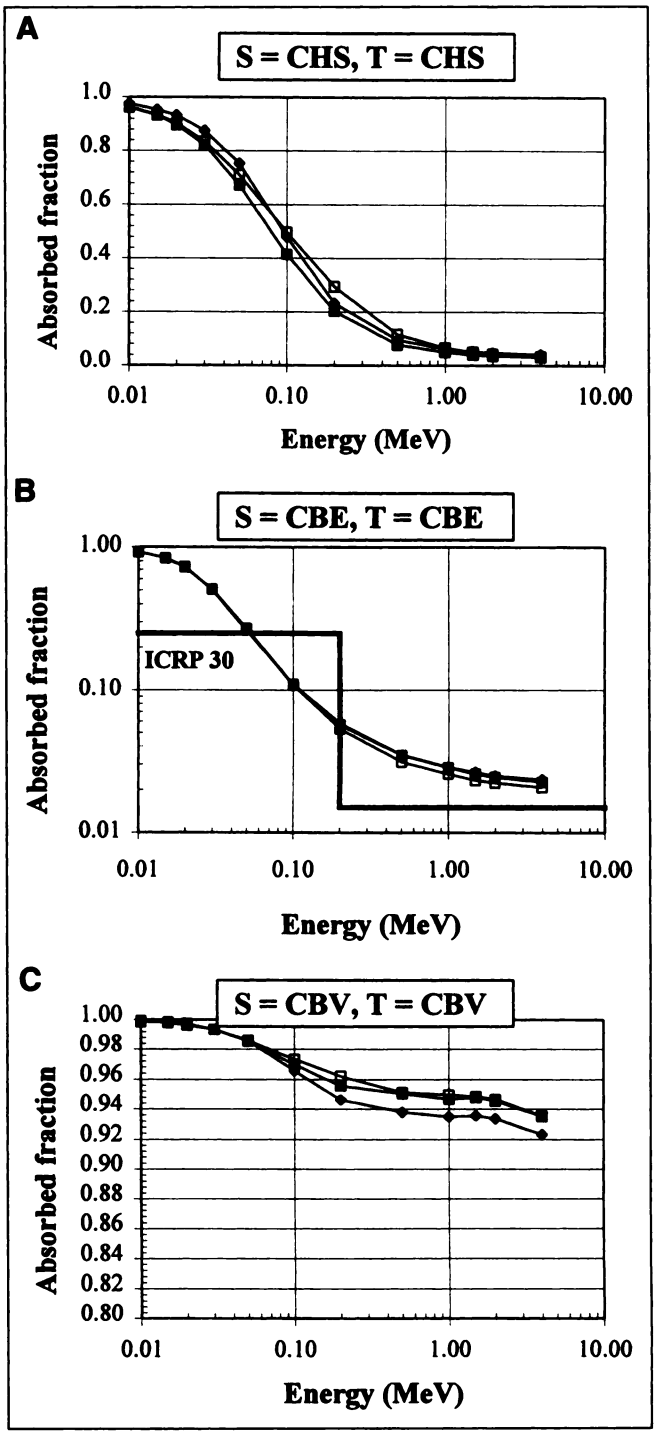

FIGURE 4. Self-absorbed fraction of energy for monoenergetic electrons located in cortical haversian space (CHS) (A), cortical bone endosteum (CBE) (B) and cortical bone volume (CBV) (C). All three cortical bone sites from which chord length distributions were available are shown: cortex of femur (■), humerus (□) and tibia (◆). Note that ordinate for graph in middle of figure is given in logarithmic scale. S = source; T = target.

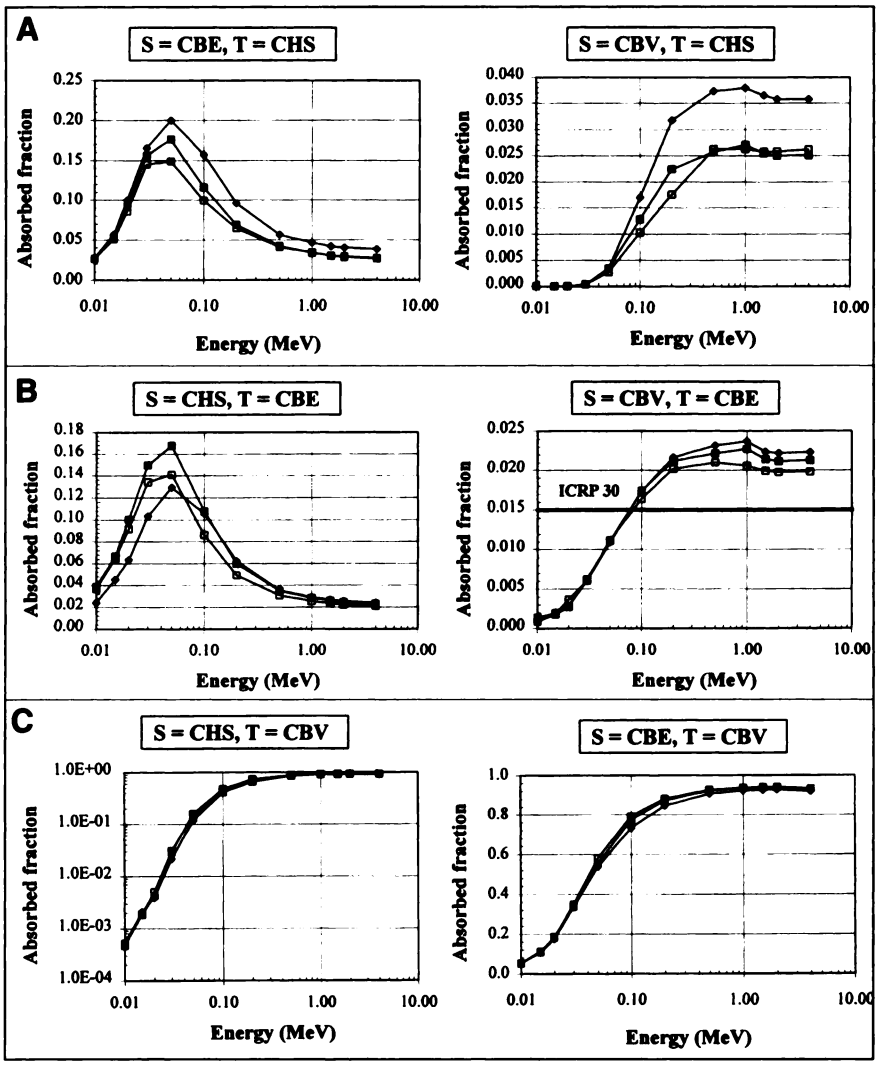

FIGURE 5. Cross-absorbed fractions of energy for monoenergetic electrons for six source (S)-target (T) combinations. Top graphs: cortical haversian space (CHS) as target and cortical bone endosteum (CBE) and cortical bone volume (CBV) as source regions. Middle graphs: CBE as target and CHS and CBV as source regions. Bottom graphs: CBV as target and CHS and CBE as source regions. All three cortical bone sites from which chord length distributions were available are shown: cortex of femur (■), humerus (□) and tibia (◆). Note that ordinate in graph at bottom left of figure (for CHS and CBE as source and target regions, respectively) is given in logarithmic scale.

absorbed fraction with bone site. The cortex of the tibia, which has the largest haversian canals, has the largest absorbed fraction at all electron source energies. When the CBE is the source (left graph, Fig. 5A), the absorbed fraction is slightly greater than zero at low electron energies because of the thinness of the endosteum. It then increases very rapidly to reach a maximum at ~60 keV. This maximum corresponds to the energy at which all electrons originating in the endosteum reach the haversian space. For higher energies, the absorbed fraction decreases as electrons start to escape the haversian space and enter the adjacent bone matrix. We see a different shape for the absorbed fraction when the source is the CBV and the target is the CHS (right graph, Fig. 5A). The absorbed fraction first starts at zero. At energies greater than ~50 keV, more electrons reach the CHS, and the absorbed fraction subsequently increases. At ~500 keV, an equilibrium is reached at which electron energy entering the CHS is equal to the electron energy exiting the CHS, and consequently, a plateau is observed in the absorbed-fraction graph.

Figure 5B shows the absorbed fraction to the CBE for the CHS and CBV as source regions. These two graphs show the same variations of the absorbed fraction that were observed for the CHS as a target because of their very small sizes compared with the bone matrix. One can also notice that the absorbed fraction to the CBE is smaller than the absorbed fraction to the CHS at all energies.

The right graph of Figure 5B for the CBE as a target and the CBV as a source also indicates the energy-independent absorbed fraction of 0.015 recommended in ICRP publication 30 for this particular source-target combination. The ICRP 30 model is shown to greatly overestimate the absorbed fraction to cortical endosteum at energies less than ~90 keV. At 10 keV, the ICRP 30 value is a factor of ~15 greater than that predicted by the current model. At high electron energies, the current model predicts absorbed fractions higher than the ICRP 30 value, but only by factors ranging from 1.3 to 1.5.

The absorbed fraction to the CBV is represented in Figure 5C for the CHS and CBE as source regions. There are almost no variations of the absorbed fraction with the cortical bone site caused by the small differences in the chord length distributions. There are also very different variations of the absorbed fractions with energies from those observed previ-

ously for the CHS and CBE as target regions. The bone matrix volume represents ~95% of the cortical bone (Table 1). Therefore, once an electron enters the bone, it will deposit almost all its energy within this region. This explains the continuous increase of the absorbed fraction with increasing energy, plateauing at ~500 keV. This increase is more abrupt for the CBE as a source (directly adjacent to the bone) than for the CHS.

CONCLUSION

A model of electron transport in cortical bone has been presented. This model extends to cortical bone a model of electron transport comparable with that developed for trabecular bone as previously published (*2*). The model uses the transverse chord length distributions through haversian cavities and bone matrix measured by Beddoe (*3,5*). This model takes into account the nonlinear trajectory of the electrons, the full transport of the electrons with δ-rays and bremsstrahlung, the distribution of sizes of haversian canals and the possibility of cross-osteon irradiation at high electron energies.

Using the electron transport code EGS4-PRESTA, absorbed fractions of energy for monoenergetic electrons are tabulated for 12 energies, considering all source and target regions in the cortical bones. The three available chord length distributions are used for this purpose. Because these chord length distributions are only for the long bones, an average of the calculated absorbed fractions is also tabulated for use with other cortical bone sites.

The possible escape of the electron from the cortical bone is not fully considered in the present model. Bremsstrahlung photons are limited to a distance of 5 cm from the starting source region, and a 2% energy escape is seen at 4 MeV. No attempt is made to simulate the real outer shape of these long bones. Therefore, the absorbed fractions presented here will overestimate slightly the true absorbed fractions, especially at high electron energies and for thin sections of cortical bones (as in the cortex of the femur head and neck, for example).

Considering that the dose to the endosteum is necessary for the calculation of effective dose (*18*), and because 40% of the mass of endosteum is located in the cortical bone (*19*), it is important to precisely calculate the dose to the cortical endosteum even in nuclear medicine applications. This electron transport model and its corresponding calculated absorbed fractions of energy will help in the accurate determination of endosteal dose. Furthermore, radionuclides injected intravenously will remain in the blood for a certain time and therefore will be seen within the haversian canals. These newly calculated absorbed fractions will allow for the dose from haversian canal sources to be more accurately calculated than in existing models.

ACKNOWLEDGMENTS

This work was supported in part by U.S. Department of Energy grant DE-FG05–95ER62006 and the Health Physics Faculty Research Award Program administered by the Oak Ridge Institute for Science and Education. Dr. Bouchet is the recipient of the Burton J. Moyer Memorial Health Physics Fellowship.

REFERENCES

1. International Commission on Radiological Protection. *A Review of the Radiosensitivity of the Tissues in Bone.* Report 11. Oxford, UK: Pergamon; 1968.
2. Bouchet LG, Jokisch WJ, Bolch WE. A three-dimensional transport model for determining absorbed fractions of energy for electrons within trabecular bone. *J Nucl Med.* 1999;40:1947–1966.
3. Beddoe AH. *The Microstructure of Mammalian Bone in Relation to the Dosimetry of Bone-Seeking Radionuclides* [dissertation]. Leeds, UK: University of Leeds; 1976.
4. International Commission on Radiological Protection. *Recommendations of the ICRP.* Report 26. Oxford, UK: Pergamon; 1977.
5. Beddoe AH. Measurements of the microscopic structure of cortical bone. *Phys Med Biol.* 1977;22:298–308.
6. Bielajew AF, Rogers DWO. PRESTA, the "parameter reduced electron step transport algorithm" for electron Monte Carlo transport. *Nucl Instr Meth.* 1987;B18:165–181.
7. Nelson WR, Hirayama RH, Roger DWO. *The EGS4 Code System.* Report 265. Palo Alto, CA: Stanford Linear Accelerator Center; 1985.
8. Darley PJ. *An Investigation of the Structure of Trabecular Bone in Relation to the Radiation Dosimetry of Bone-Seeking Radionuclides* [thesis]. Leeds, UK: University of Leeds; 1972.
9. Whitwell JR. *Theoretical Investigations of Energy Loss by Ionizing Particles in Bone* [thesis]. Leeds, UK: University of Leeds; 1973.
10. Whitwell JR, Spiers FW. Calculated beta-ray dose factors for trabecular bone. *Phys Med Biol.* 1976;21:16–38.
11. Akabani G. Absorbed dose calculations in Haversian canals for several beta-emitting radionuclides. *J Nucl Med.* 1993;34:1361–1366.
12. International Commission on Radiation Units and Measurements. *Stopping Powers for Electrons and Positrons.* Report 37. Bethesda, MD: International Commission on Radiation Units and Measurements; 1984.
13. International Commission on Radiological Protection. *Recommendations of the International Commission on Radiological Protection.* Publication 26. Oxford, UK: Pergamon; 1977.
14. Coleman R. Random paths through convex bodies. *J Appl Prob.* 1969;6:430–441.
15. Eckerman KF, Ryman JC, Taner AC, Kerr GD. Traversal of cells by radiation and absorbed fraction estimates for electrons and alpha particles. In: Schlafke-Stelson AT, Watson EE, eds. *Proceedings of the Fourth International Radiopharmaceutical Dosimetry Symposium.* CONF-851113. Oak Ridge, TN: Oak Ridge Associated Universities; 1985:67–81.
16. Kellerer AM. Considerations on the random traversal of convex bodies and solutions for general cylinders. *Radiat Res.* 1971;47:359–376.
17. International Commission on Radiation Units and Measurements. *Photon, Electron, Proton and Neutron Interaction Data for Body Tissues.* Report 46. Bethesda, MD: International Commission on Radiation Units and Measurements; 1992.
18. International Commission on Radiological Protection. *1990 Recommendations.* Publication 60. Oxford, UK: Pergamon; 1991.
19. International Commission on Radiological Protection. *Basic Anatomical and Physiological Data for Use in Radiological Protection: the Skeleton.* Publication 70. Tarrytown, NY: International Commission on Radiological Protection; 1995.